Petroleum Science 20 (2023) 2512–2520

Contents lists available at ScienceDirect

Petroleum Science

journal homepage: www.keaipublishing.com/en/journals/petroleum-science

Original Paper

Unraveling the influence of surface roughness on oil displacement by Janus nanoparticles

Yuan-Hao Chang, Sen-Bo Xiao**, Rui Ma, Zhi-Liang Zhang, Jian-Ying He*

Department of Structural Engineering, Norwegian University of Science and Technology (NTNU), 7491, Trondheim, Norway

ARTICLE INFO

Article history:
Received 9 May 2022
Received in revised form
27 July 2022
Accepted 13 February 2023
Available online 21 February 2023

Edited by Jia-Jia Fei and Teng Zhu

Keywords:
Janus nanoparticles
Oil displacement
Enhanced oil recovery
Molecular dynamics simulation
Rough surface

ABSTRACT

Janus nanoparticles (JNPs) possess great potential in recovering the residual oil from reservoirs, however, the fundamental interaction mechanisms among nanoparticles, the oil, and reservoir wall characteristics remain to be elucidated. In this work, models of oil trapping grooves with different geometric features are subjected to molecular dynamics simulations for investigating the influences of roughness parameters on oil displacement dynamics by JNPs. Four key surface geometry parameters and different degrees of surface hydrophobicity are considered. Our results indicate that JNPs hold an outstanding performance in displacing residual oil on weakly to moderately hydrophobic surfaces. Overall, smaller entry and exit angles, the larger aspect ratio of the oil trapping grooves, and a bigger tip length of the rough ridges lead to superior oil recovery. Among the key geometric parameters, the aspect ratio of the oil trapping grooves plays the dominant role. These insights about the interaction of surface properties and JNPs and the resulting trapped oil displacement could serve as a theoretical reference for the application of JNPs for targeted reservoir conditions.

1. Introduction

Being the greatest part of global energy, the demand for fossil fuels will grow by more than 30% in 20 years (Qian and Li, 2018). Since most oil fields have reached the economic limit of the secondary oil recovery stage, the implementation of enhanced oil recovery (EOR) measures is the key to meeting the oil consumption demand (Li et al., 2000; Jia, 2020). Taking Norway as an example, a merely 1% recovery increase in the EOR stage will translate into more than 300 billion Norwegian kroner in revenue. Currently, the traditional EOR technology has entered a bottleneck period due to challenges like high cost, eco-unfriendliness, and gravity override (Sun et al., 2015; Chang et al., 2016; Kang et al., 2020). In the meanwhile, nanoparticles have been widely accepted to have great potential to be a breakthrough in EOR (Liang et al., 2021; Sun et al., 2021; Zhang et al., 2022). In particular, there is growing interest in the EOR application of Janus nanoparticles (JNPs) whose surfaces have two distinct wettability (Shi et al., 2019; Wu et al., 2020b; Jia et al., 2021).

There is a bulk of encouraging results indicating that JNPs exhibit significantly better performance and greater application potentials than conventional homogeneous nanoparticles in the EOR process (Luo et al., 2016; Liang et al., 2017; Giraldo et al., 2019; Yin et al., 2019; Li et al., 2020; Liu et al., 2020; Wu et al., 2020a). Through experimental studies, JNPs were found to contribute to water viscosity increment (Giraldo et al., 2019), interfacial tension reduction (Wu et al., 2020a; Yin et al., 2021), and surface wettability alteration (Giraldo et al., 2019; Wu et al., 2020a) in the EOR process. Moreover, JNPs exhibited a special dynamic displacement mechanism of climbing film growth and slug-like displacement that was not observed in other homogeneous nanoparticles (Luo et al., 2016). What's more, the simulation study provides the theoretical fundamentals of JNPs in EOR technology (Zhao et al., 2019; Ahmadi and Chen, 2021), which effectively compensates for the current limitation of experimental conditions at the nanoscale. For example, the interfacial activities of JNPs at the oil-water interface were explored by dissipative particle dynamics (DPD) simulations, yielding results for the design of the Pickering emulsion (Luu and Striolo, 2014). The self-assembly and characteristics of JNPs at the oil-water interface were studied by molecular dynamics (MD) simulations, which supplied the basis of JNP applications in practice

* Corresponding author.
** Corresponding author.
E-mail addresses: senbo.xiao@ntnu.no (S.-B. Xiao), jianying.he@ntnu.no (J.-Y. He).

https://doi.org/10.1016/j.petsci.2023.02.006

(Xiang et al., 2017). Due to the size limitation of these simulation systems, only a limited number of nanofluid flooding systems involving solid surfaces exist. Unexpected results of JNPs impeding oil displacement were observed in capillary pressure-dominated smooth nano-channels (Wang et al., 2019). The great potential of JNPs in displacing residual oil from rough channels was also newly reported (Chang et al., 2022a). Moreover, the outstanding performance of JNPs and their unique dynamics of the wettability alteration process (namely, the 'adsorption invasion process') were revealed (Chang et al., 2022b). Obviously, these limited works are far from the complete understanding of displacing trapped oil in reservoir pores and throats with JNPs.

It is worth noting that the significantly different results in smooth and rough nanochannels highlight the influence of roughness in oil displacement dynamics (Niu and Tang, 2014; Zhang, 2016; Wang et al., 2019). Besides, differences in flow and wetting characteristics of nanofluids on smooth and rough surfaces have been confirmed in studies in varied research fields (Savoy and Escobedo, 2012; Wang et al., 2017; Durret et al., 2018). Hence, only by taking into account the roughness effect of solid surfaces (the actual reservoir situation), the motion law of JNPs, the oil displacement effect, and the EOR mechanism can be more truly manifested. Considering the size limitation of molecular simulation systems, it is nevertheless challenging to construct the real rough topography in the oil reservoir. Generally, surface roughness is featured by grooves with regular shapes in MD simulations (Yaghoubi and Foroutan, 2018; Fang et al., 2019). By modifying the geometric parameters of the grooves, the influence of the surface roughness on fluid dynamics or wetting can be effectively elucidated (Xie and Cao, 2016; Song et al., 2018; Fang et al., 2019). Regrettably, there are seldom molecular simulation studies on the influence of nanochannel roughness on oil displacement.

Herein, the effects of surface geometric parameters on displacing oil from nano-pockets are investigated. Specifically, the tip length of the ridge (S), entry angle (α), exit angle (β), and the aspect ratio (A) of the groove width (L) to depth (H) (that is, A=L/H), as shown in Fig. 1, are chosen as the focused roughness parameters. As the most common geometric parameters in research on the rough surface (Lalegani et al., 2018; Fang et al., 2019), their combinations are able to cover almost all the rough surface geometry. By monitoring the formation of JNPs adsorption film on the sidewall of the grooves and comparing the final oil displacement results, the EOR effect of each surface geometric parameter is quantitatively analyzed and clarified. Moreover, an in-depth discussion on the possible interactive influence among the geometric parameters and the limitation of this work is conducted. The results broaden the understanding of the adaptability of JNPs in displacing residual oil on rough surfaces and are thus desired by the application of JNPs in EOR.

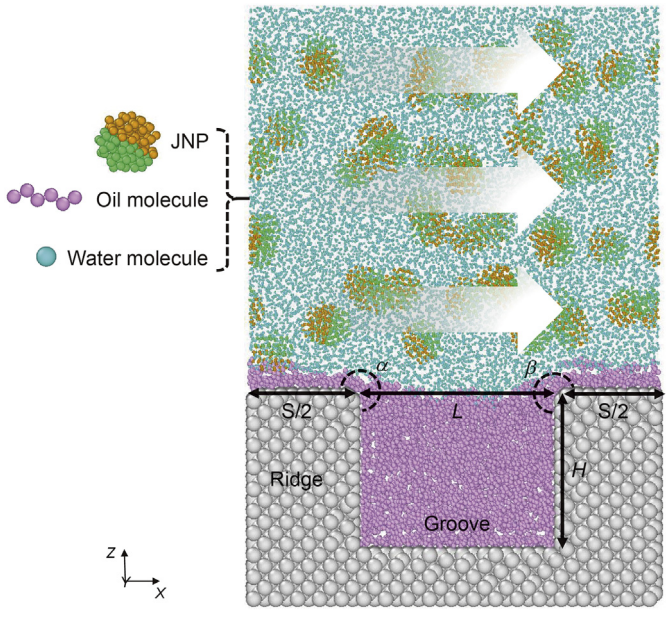

Fig. 1. Representative structure of the simulation system. The white arrows indicate the flooding direction in the periodic simulation box. The colors for different components in the system: water (light blue), oil (pink), surface (grey), hydrophobic part (orange), and hydrophilic part (green) of Janus NPs. The key geometric parameters, the tip length of the ridge (S), entry angle (α), exit angle (β), groove width (L), and depth (H) are illustrated in the figure.

2. Model and simulation details

2.1. Molecular model

The model systems are constructed with the aim to capture the key features of rough surfaces with trapped oil for displacement by the injection of JNPs, as one representative example shown in Fig. 1. Following previous studies and for the sake of simplicity (Chang et al., 2022b), the model systems hold a dimension of $100 \times 70 \times 151$ Å^3 with periodic boundary conditions. The rough surface is created by removing atoms from an initially smooth silicon crystal to result in a groove, as represented by a rectangular groove in Fig. 1. The hydrophobicity of such surface is controlled by its inter-atomic interactions with the water and oil phase, namely the force-field parameters, which could capture the wetting features of common types of rocks found in actual reservoirs (Kondratyuk et al., 2005; Harrison et al., 2014). To avoid artificial molecular interactions across the solid surface because of the periodic boundary condition, the minimum height at the bottom of the groove in the surface (11 Å) is set to be larger than the cutoff distance of the non-bonding interactions (10 Å). The crucial geometric parameters of the surface roughness, namely the tip length of the ridge (S), entry angle (α), exit angle (β), and the aspect ratio of the groove (A) as depicted in the figure, are altered in surface modeling, with the chosen values listed in Table 1. As such, multiple systems with varied rough surfaces are obtained for the oil displacement simulations. It is worth noting here that the system containing a rough surface with $S = 50$ Å, $\alpha = 270°$, $\beta = 270°$ and $A = 1.25$ is taken as the reference for result comparison, as highlighted in the bold text in Table 1. For the fluid of the model systems, hexane (model density 660 kg/m^3), water, and spherical JNPs with diameters of 10 Å ($d = 10$ Å) are used. As an example, the reference system contains 1001 oil molecules, 21400 water molecules, and 48 JNPs with a nanoparticle volume concentration of 3.9%. The JNPs are evenly distributed in the solution before flooding simulation in an equilibrium state.

2.2. Force field

The atomistic interaction parameters are selected following previous studies. Specifically, the monoatomic water (mW) model is adopted for the water phase, while the Transferable Potentials for Phase Equilibria united-atom (TraPPE-UA) description of hexane is employed for oil (Martin and Siepmann, 1998; Molinero and Moore, 2009). The mW water models interact via the 3-body Stillinger-Weber (SW) potential to account for the hydrogen bonding in water. The water-oil and oil-oil non-bonded interactions follow the standard pairwise 12-6 Lennard-Jones (LJ) potential. The combination of the water and oil models is found to appropriately capture the fluid properties at minimal computational costs (Chang et al.,

Table 1
The selected geometric values in modeling the rough surfaces. The bold values are the parameters of the reference model.

Geometric Parameters	Designed Value						
Tip Length of the Ridge (S) (d=10 Å)	2.5d	3d	4d	**5d**		7.5d	10d
Entry Angle (α)	210°	225°	240°	**270°**		300°	315°
Exit Angle (β)	210°	225°	240°	**270°**		300°	315°
Aspect Ratio of the groove (A)	0.625	**1.250**	1.875	2.500	3.125	3.750	5.000

2021). The interactions between the surface with water and oil are also parameterized by LJ potentials, with the oil droplet contact angle on the surface controlled by the characteristic energy ε_{sw} (water-surface), as depicted in Fig. S1. Since the focus is the influence of the morphology of rough surface rather than the specific materials of the surface, the choice of the ε_{sw} is to guarantee the oil phase trapped in the groove on the surface for flooding, as detailed in the follow sections. The characteristic energy for interactions involved the JNPs is selected from the previous studies (Chang et al., 2022b), with the values given in the supporting information (Table S1). Although the atoms in the systems are free of charge, the effect of coulombic interactions in the system, especially among the water molecules, are implicitly accounted for by the adopted water model and the force field.

2.3. Simulation strategy and process

All the MD simulations are performed with the LAMMPS package (Plimpton, 1995) and visualized with OVITO software (Stukowski, 2009). In our simulations, the systems are first energy-minimized using the steepest descent method and followed by a 5-ns equilibrium stage in the NVT ensemble at 350 K. The simulation time step is 3 fs. The Nosé–Hoover thermostat with a coupling coefficient of 100 fs is adopted in the simulations (Hoover, 1985). After then, another 60-ns non-equilibrium MD simulation (NEMD) is carried out to simulate the JNP flooding process, with a constant force (0.01 kcal mol^{-1} Å^{-1}) applied on each of the water molecules along the x-axis of the simulation box. To speed up the simulation of such big systems, rigid JNPs are chosen. As such, any result obtained here in this work applies to relatively rigid nanoparticles used in EOR. At the same time, the rough surface is positionally fixed. Five independent simulations are carried out for the flooding process in each system.

3. Results

3.1. Oil displacement dynamics on the rough surface by JNPs

It is known that local wettability alteration is one of the major mechanisms in residual oil displacement by JNPs. Especially, the dynamic 'adsorption invasion process' in wettability alteration was identified to be the main motion pattern of the JNPs in the oil displacement (Chang et al., 2022b), as schematically illustrated in Fig. 2. Because of their special surface wettability, JNPs are prone to adsorb at the oil-water interface and onto trapped oil films on rough surfaces. Under the shear flow of the flooding water, JNPs slide on the surface and then linger at the edge of oil trapping grooves because of the pinning effect. Driven by the local water currents, the accumulated JNPs at the edge of the groove are able to invade the entrance of the groove along the sidewall of the groove to displace the trapped oil. The sequential events of JNPs adsorption and invasion result in many JNPs progressing into the deeper position of the groove, forming a JNP adsorption film along the sidewall of the groove and altering the local wettability to be more hydrophilic. The above whole process contributes to the outstanding performance of JNP in displacing residual oil. It is obvious that the important properties of the adsorption JNP film, for instance, the height of the film and the orientation of the adsorbed JNPs, determine the final EOR effect.

The excellent displacement effects on the trapped oil from the rough surface by JNPs thus call for the further unfolding of the influences of the surface morphology parameters. In order to effectively probe the surface wettability and the resulting trapping strength of oil in the grooves of the rough surface, equilibration simulations of oil droplets adsorption on surfaces with varied LJ interaction characteristic energy with water are carried out, as shown in Fig. S1. The surfaces with ϵ_{sw} in the range of 0.1–0.5 kcal/mol cover the wettability being strongly hydrophobic to weakly hydrophilic. Within this wettability range, trapped oil displacement from the groove on these surfaces by JNP is then performed, with the resulting system snapshots of each simulation collected in Fig. 3a. Clearly, varied surface wettability (ϵ_{sw}) leads to differences in the amount of retained residual oil and the adsorption JNP film formed on the sidewall of the groove. In order to quantify the oil displacement effect, the percentage of displaced oil molecules (EOR), averaged JNP invasion depth into the groove (D, that is the averaged absolute coordinate of the adsorbed JNP), and the hydrophilic ratio of adsorbed JNP facing off the sidewall of the groove (as shown in Fig. S2, $R_{hydrophilic}$ is defined as the ratio of the volume of the hydrophilic beads in the half of NPs away from the surface, representing the degree of surface wettability alteration by individual JNP), are calculated and shown in Fig. 3b. For surfaces ϵ_{sw} in the range of 0.25–0.40 kcal/mol, which approximately corresponds to weak to moderate hydrophobicity, EOR is found to maintain at a

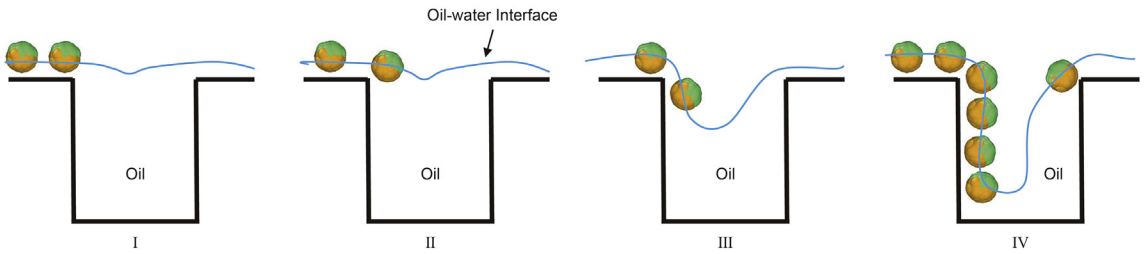

Fig. 2. Schematic diagram of the 'adsorption invasion process' of JNPs in the flooding. From left to right are I oil-water interface identification and surface adsorption, II edge pinning, III invasion, and IV formation of adsorption film.

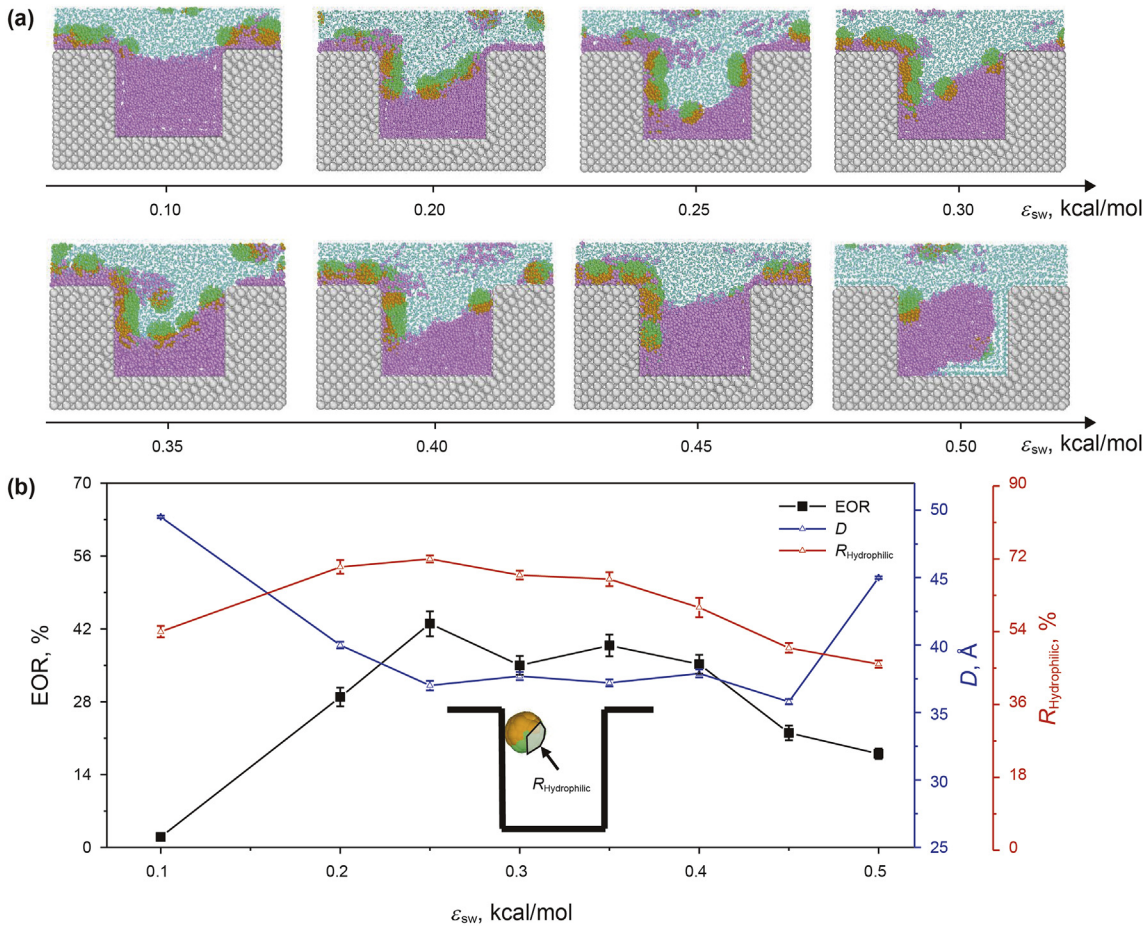

Fig. 3. The effect of surface wettability on oil displacement. (**a**) The final system snapshots after oil displacement on surfaces with varied ϵ_{sw}. (**b**) The resulting EOR, D and $R_{hydrophilic}$ obtained after the simulations. The error bar indicates the standard deviation of 5 independent simulations. The inset indicates the definition of the $R_{hydrophilic}$ of the JNPs on the sidewall of the groove.

higher level. The $R_{hydrophilic}$ shares a similar trend with that of the EOR effect, which suggests the differences in the orientation of the JNPs in the adsorption film on the sidewall of the groove correlate and underpin the different EOR effects. For both the low- and high-end values of ϵ_{sw}, low EOR is associated with high values of D, meaning JNPs cannot effectively invade the groove. When the surface is strongly hydrophobic (low ϵ_{sw}), oil is firmly trapped in the groove owing to the hydrophobic effect making it difficult for JNPs to adsorb and invade the groove along the surface; when the surface is hydrophilic (high ϵ_{sw}), the adsorption of JNPs at the entrance cannot efficiently form an adsorption film to guide water entering into the groove. Therefore, JNPs are suitable for displacing residual oil on rough surfaces with weak to moderate hydrophobicity. To clarify the rough geometric effects, surfaces with ϵ_{sw} of 0.3 kcal/mol (i.e. weak hydrophobic surface) are selected for further simulations.

3.2. Effects of the surface geometric parameters

In the simulation, the rough surface is simplified as a combined unit of the groove and the ridge. The rough surfaces with different geometric characteristics can thus be designed by modifying the four key geometric parameters (tip length of the ridge (S), entry angle (α), exit angle (β), and aspect ratio of the groove (A)). Based on the oil displacement dynamics by JNPs, it can be expected that varied geometric parameters will affect the specific process of JNP's 'adsorption invasion process'. Therefore, apart from the EOR effect, the quality of the JNP adsorption film on the sidewall (the amount, depth, and orientation of the adsorbed JNPs) should also be the focus of the following study.

3.2.1. Tip length of the ridge (*S*)

In the 'adsorption invasion process', JNPs obtain the initial contact with the surface by identifying the oil film on the plane surface, namely loading on the ridges of the rough surface topography. As such, the larger S, the more adsorbed JNPs on the surface. Subsequently, there can be possibly more JNPs entering inside the groove along the sidewall and a stronger driving force for the deepening of the progressing adsorption film. Indeed, as shown in Fig. 4a, a small value of S (2.5d) leads to the few adsorbed JNPs on the sidewall and low oil displacement performance of the JNPs (the snapshots are shown in Fig. S3). With the tip length slightly increasing from 2.5d to 3d, obvious JNPs adsorption film gradually penetrates downward into the groove with significant oil being displaced outside the groove. However, both EOR and D confirm that the change in oil displacement effect weakens when S is over 3d. Such results imply that there is a threshold of S for the massive adsorption of JNPs onto the rough surface. Once S reaches this length threshold, the average depth of invading JNPs adsorption film as well as the subsequent EOR effect will reach stable results. In our case, the threshold of S is three times the diameter of the JNPs (3d). The above results suggest that rough surfaces with sharp ridges could be unfriendly for JNPs in EOR in the real reservoir.

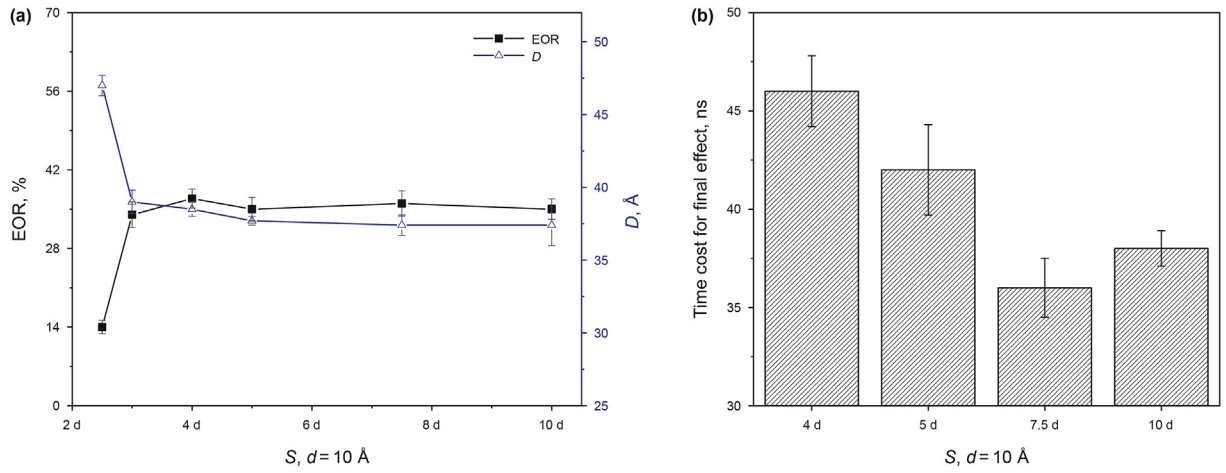

Fig. 4. The effect of the tip length of the ridge, *S*, on the oil displacement. (**a**) The EOR and the depth of adsorption film, *D*, obtained in systems with varied *S*. (**b**) The time needed for reaching the final stable EOR effect in the system with varied *S*. The error bars in the figures are the standard deviation of 5 independent simulations.

What's more, the *S* also has an obvious influence on the time cost for obtaining the final EOR effect. As exemplified by the systems with the similar EOR effect (*S* ranging from 4*d* to 10*d*) shown in Fig. 4b, larger *S* generally requires a shorter time of the displacement process. The high value of *S*, meaning long plane surface, is a favorite for speeding up the acquisition of the high level of EOR. Of course, if *S* is extremely long, the sliding distance of the adsorbed JNPs will increase, which may slow down the EOR process to a certain extent. As such, the system with *S* of 10*d* shows an increase in needed displacement time to its counterpart with *S* of 7.5*d* (Fig. 4b).

3.2.2. Entry angle (α)

The effect of α on oil displacement is obvious by comparing the final simulation system snapshots, as shown in Fig. 5a. It should be noted here that to ensure the same width of the groove (*L*), the depth of the groove (*H*) reduces if the α reaches a low value. For example, the *H* in the system with α of 210° is smaller than that in other systems (Fig. 5a). Considering that the sidewall area is no longer the same among the systems, the surface coverage ratio (φ) of adsorbed JNPs on the sidewall (that is, the ratio of the area covered by the adsorbed JNPs) is chosen to characterize the effectiveness of the adsorption film here. As the results of EOR, φ and $R_{\text{hydrophilic}}$ shown in Fig. 5b, lowering the α generally leads to a better oil displacement effect. The resulting φ and $R_{\text{hydrophilic}}$ share a highly similar trend at varied α, suggesting a strong correlation. In conclusion, α affects the amounts and the orientation of the adsorbed JNPs on the groove sidewall. Favorite properties of the adsorption film, namely high values of φ and $R_{\text{hydrophilic}}$, lead to a preferable oil displacement effect.

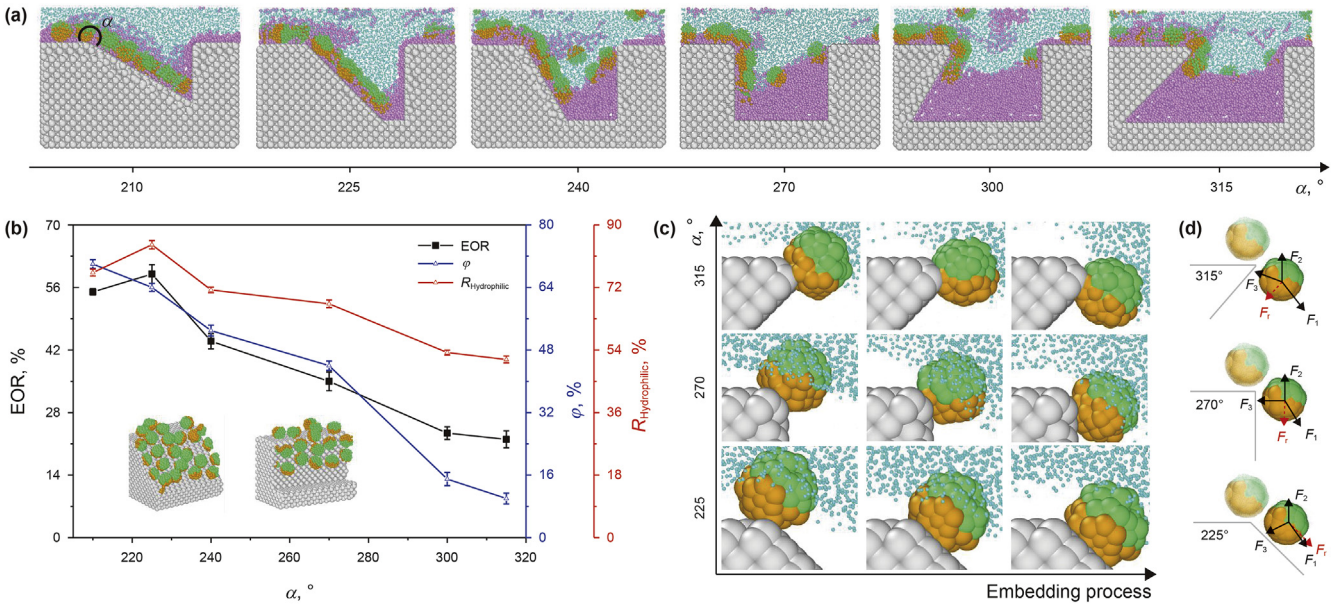

Fig. 5. The effect of entry angle on oil displacement. (**a**) The final system snapshots of oil displacement in grooves with varied entry angles. (**b**) The EOR, the surface coverage ratio, φ, and $R_{\text{hydrophilic}}$ with varied entry angles. Two snapshots of two representatives of adsorption films on the sidewall of the groove are shown as insets. Error bars are standard deviations of 5 independent simulations. (**c**) Progressing snapshots of JNPs at the entrance of grooves with three different entry angles. (**d**) The schematic of forces on the JNPs at the entrance of grooves. The black arrows represent component forces while red arrows indicate the resultant forces. F_1 represents the collision force asserted on the JNPs. F_2 is the resisting force of JNPs interacting with the oil molecules. F_3 represents the attraction force from the surface to the JNP. F_r is the net driving force on the JNP to enter the groove.

The above results obviously indicate that α affects the dynamics of JNPs pinned at the entrance of the groove and is about to slide onto the groove sidewall. As the representative JNPs at the entrance of the groove with three different α monitored and shown in Fig. 5c, the JNPs are similar in orientations but subjected to the different driving forces in collision with other adsorbed JNPs. Because of the different α, the directions of forces applied to the JNPs at the entrance of the groove are different. As shown in Fig. 5d, the effective force driving JNPs into the groove (F_r, Fig. 5d) is more inline with the important collision force (F_1, Fig. 5d) at lower α. F_r increases as α decreases, which enhances JNPs to enter and invade the groove. This explains the change in the coverage ratio of JNP shown in Fig. 5b. Although the JNPs can adjust the orientation through self-rotation during the simulation under the influence of the interactions between surface, water, and oil, the improvement of the $R_{hydrophilic}$ is limited in the whole displacement process, giving the same results as previous studies (Chang et al., 2022b). The initial orientation of the pinned JNP at the entrance of the groove largely reflects the final $R_{hydrophilic}$ of the adsorption film. In summary, smaller α leads to the favorite initial orientation of the pinned JNPs, and the final larger $R_{hydrophilic}$.

3.2.3. Exit angle (β)

The exit angle of the groove, β, is also crucially important to the oil displacement results. Compared to the entering sidewall of the groove, the other sidewall facing the flooding direction (the outlet side) has very limited action with the JNPs during the oil displacement process. As the snapshots shown in Fig. S4a, the uncovered trapped oil at the outlet side increases. Specifically, the increase of β leads to a decrease in the recovery efficiency of the oil phase given adsorption JNPs film with similar effectiveness in the groove, as shown in Fig. S4b. In addition, it should be mentioned that the increase of β also eliminates the possibility of JNP adsorption on the sidewall of the groove facing the direction of flooding, which is not conducive to the expansion of the oil-water interface morphology inside the oil-trapping groove.

3.2.4. Aspect ratio of the groove (A)

The aspect ratio of the groove, A, was found to be an important roughness factor in oil extraction by gas flooding (Fang et al., 2019). Here, the width of the groove changes from 2.5 to 20 times the diameter of JNPs, while the height of the grooves is constant. The corresponding A of the grooves in the system ranges from 0.625 to 5. The varied A of grooves leads to significant differences in the final oil displacement results, as the EOR, φ and $R_{hydrophilic}$ shown in Fig. 6a (the snapshots are plotted in Fig. S5). Overall, an increase of A leads to an increase in EOR in the systems. Although varied A has a limited effect on the orientation of adsorbed JNPs, it results in the changes in adsorption film coverage, φ, showing a pattern of positive correlation (blue curve, Fig. 6a). As verified already by results in former studies (Chen et al., 2017; Fang et al., 2019), the water flow pattern at the oil-water interface can be more concave with the enlargement of the groove width, as shown by the schematics in Fig. 6b. The larger the aspect ratio, the deeper the downward thrust of the water flows over the groove. The curved oil-water interface on the groove with large A is a favorite for the local fluid flow to exert a driving force on the pinned JNPs at the entrance of the groove, enhancing the invasion of JNPs into the groove along the sidewall and forming the JNPs adsorption film. Nevertheless, the EOR still witnesses significant changes in the periods of stable coverage ratio ($A = 1.25–2.5$ or $A = 3.125–3.75$). This implies that the impact of the aspect ratio of the groove is not only in the coverage area of the adsorption film.

It can be inferred that once the formation of a JNP adsorption film on the sidewall of the groove, namely the local wettability of the sidewall is altered, the influence of A on the oil-water interface can be even more complicated. In order to clarify the impact of the wettability alteration of the sidewall, a design system with a hydrophilic sidewall is used to further explore the effect of A on oil recovery results and the morphology of the oil-water interface. As the schematic diagram shown in Fig. S6, the sidewall in systems is modified to be partially water wet and share the same properties as the hydrophilic face of the JNPs before the displacement. The hydrophilic parts of the sidewalls in these designed grooves have a fixed height, namely 30 Å on the entering sidewall representing altered wettability and 3 Å on the exiting sidewall also mimicking coverage of JNPs. Meanwhile, the rest of the groove remains hydrophobic, with a ε_{sw} of 0.3 kcal/mol. The hydrophilic parts of the grooves in the designed systems are then considered to have been covered by JNP adsorption film. The designed systems are then subjected to a flooding test by pure water to probe the effect of altered wettability in the grooves, with the EOR results shown in Fig. 6c and resulting final system snapshots after oil displacement in Fig. S7. Interestingly, as A increases, the EOR slightly decreases first with a minimum near $A = 2.5$ and further followed by a significant increase with large A values. Such a result is coincident with the EOR results obtained in the reference group (using JNPs) and shown in Fig. 6a. As the morphology of the oil-water interface in the designed systems after oil displacement is shown on the left side of Fig. 6d, obviously, the larger A, the more curved the oil-water interface towards the bottom of the groove. Combined with the results shown in Fig. 6c, it can be seen that the dramatic concave of the oil-water interface in grooves with $A > 2.5$ underlies the high EOR performance in these systems. The designed system shed light on the understanding of the results obtained using JNPs. As the corresponding morphology of the oil-water interface obtained by JNPs for comparison shown on the right side of Fig. 6d, the general pattern of the oil-water interface in the reference systems is the same as that in the designed systems. The results significantly confirm the function of surface wettability alteration of JNPs, which is an important contributing factor to consider in EOR materials design.

To be concluded, the change of the initial streamline at the oil-water interface caused by varied A affects the coverage of the adsorption film on the sidewall of the groove. Also, the formation of the adsorption film transforms the morphology patterns of the oil-water interface in the groove with different A. The synergy of the two effects defines the final oil displacement efficiency.

4. Discussion

The above results elaborate on the influence of four important geometric parameters of rough surface on the residual oil displacement by JNPs separately. The resulting EOR and the underlying function of each geometric parameter are summarized in Table 2. Inevitably, there is synergy among the four parameters in their EOR effect. Since S characterizes the area size for the adsorption of JNPs on the surface and further determines the formation of the adsorption film inside the groove, the small value of α (close to 180°) can contribute to the effect of S, given that the entrance of the groove with small α partially can serve as an extension of the JNPs adsorption area. Namely, the entrance of the grooves with small α features the flat surface plane of the ridge with a low thickness of the trapped oil, where JNPs can be directly adsorbed at this entrance area of the groove by identifying the oil-water interface. As such, the lower threshold of S is needed for the obvious EOR effect by JNPs in grooves with smaller α. Moreover, there is the interplay of α and A because different properties of the adsorption film on the sidewall of the groove may induce different morphology of the oil-water interface in the groove and further

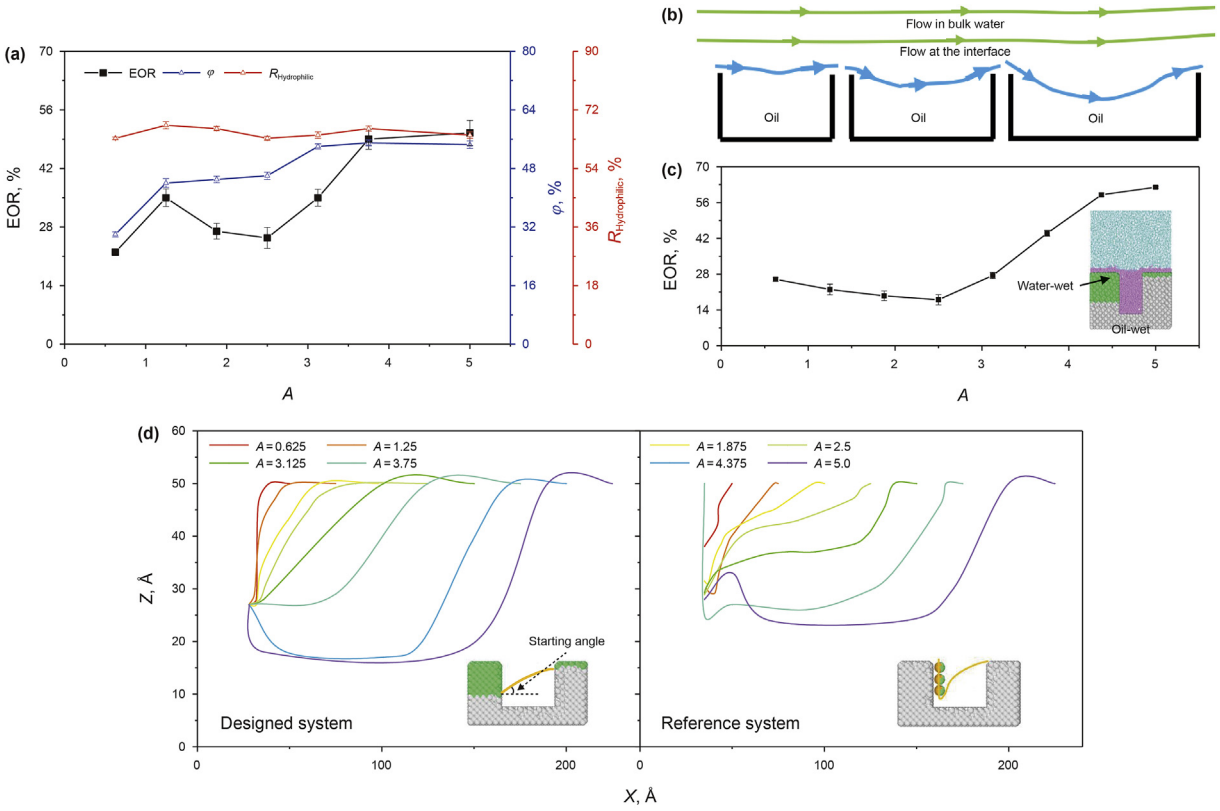

Fig. 6. The effect of the aspect ratio of the groove, *A*, on oil displacement. (**a**) The EOR, the surface coverage ratio, φ, and the hydrophilic ratio of JNPs adsorption film, $R_{hydrophilic}$, with varied aspect ratios. The error bars are the standard deviation of 5 independent simulations (**b**) The schematics of the influence of aspect ratio on streamlines at the oil-water interface monitored in previous studies. The blue ones are the water streamlines at the interface while the light green ones are that in the bulk water. (**c**) The EOR of the designed systems with various aspect ratios. The inset snapshot shows the sketch of the designed system. The green part of the designed surface is hydrophilic while the grey part is hydrophobic. (**d**) The morphology of the oil-water interface at the end of oil displacement simulations on grooves of different aspect ratios in the designed systems (left) and the reference systems (right). Inset snapshots are the representatives of the morphology of the oil-water interface in the two systems.

Table 2
The EOR effects and the underlying functions in oil displacement of the four rough geometric parameters.

Geometric Parameters	Tip Length of the Ridge (*S*)	Entry Angle (α)	Exit Angle (β)	Aspect Ratio of the groove (*A*)
Effect on EOR	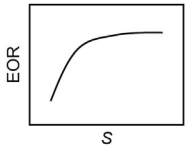	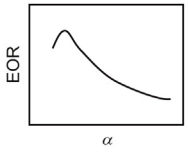	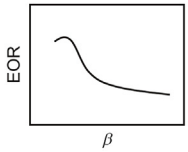	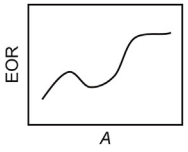
Dominating Factor in Displacement	Area of Adsorption Film	Area of Adsorption Film & Its Contribution in Wettability Alteration	Uncovered Area of Trapped Oil at Exit Side	Morphology of Oil-water Interface

lead to different EOR effects. To gain an overview of oil displacement effects, the EOR, φ and $R_{hydrophilic}$ in grooves with three entry angles of varied aspect ratios are organized in Fig. 7a. Being consistent with the results of single-parameter analysis, the system with smaller α and larger *A* holds better EOR. For any *A* and α, the properties of the JNPs adsorption film, namely φ and $R_{hydrophilic}$, determine the resulting EOR. Interestingly, for the groove with $\alpha = 300^{\circ}$ and large aspect ratio *A*, although the φ and $R_{hydrophilic}$ show very low value due to the influence of α, the corresponding EOR can still achieve a high value. This highlights the dominating effect of the meniscus of the oil-water interface in those grooves with large *A*. As shown in Fig. S8, the oil-water interface in grooves with an extraordinarily large aspect ratio can even reach the bottom of the groove. The obvious influences in the EOR effects by the exit angle are only observed in grooves with sufficiently small *A*. For grooves with a large aspect ratio *A*, the effect exit angle can become negligible since the adjacent area to the exit of the groove for trapping oil decreases proportionally. Hence, the outstanding oil displacement effect by JNPs is expected on the rough surface dominated by shallow grooves if only the tip length of the ridge exceeds a size threshold. For highly dense and deep grooves, the smaller α and β are crucial for high oil recovery efficiency by JNPs. It should be noted that if α and β are infinitely close to 180° (the surface is close to smooth), the displacement effect of JNP will be

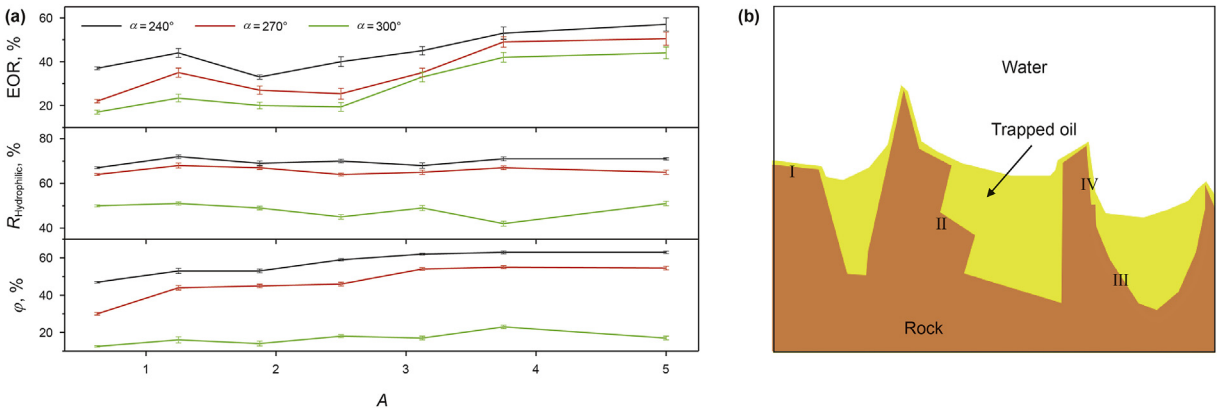

Fig. 7. The interplay of the geometric parameters in the EOR effect. (**a**) The EOR, the hydrophilic ratio, $R_{hydrophilic}$, and surface coverage ratio, φ, of the JNPs adsorption film in three grooves with different entry angles and varied aspect ratios of the groove. (**b**) Sketch of the rough surface topography with complex roughness.

poor because of the lack of pinning effect. Once the surface roughness is extremely low, results obtained in smooth channels can be applied (Wang et al., 2019).

It is worth noting that the actual topography of rough surfaces is far more complicated than the modeled groove system in the study. For example, the tip of the ridge can be a slope rather than the plane surface (I or IV, Fig. 7b); the sidewall of the groove can have a rough landscape (II, Fig. 7b); the surface is curved instead of being flat (III, Fig. 7b), and so on. However, the influence of the roughness in EOR can be deciphered using the four geometric parameters discussed above. Taking the tip of the ridge as an example, JNPs are able to land and pin on the top area of the ridge because of the hydrophobic attraction of the top oil film. In this study, the tip of the ridge is a plane surface with an inclination angle of 0°, which yields results indicating the size of the tip of the ridge should exceed the threshold to enable effective adsorption of JNPs for a favorable EOR effect. For ridges with an inclination angle lower than 0° in reality (I, Fig. 7b), the effect of a small groove entry angle can be applied, which also could reduce the size threshold of the ridge for the EOR effect. In contrast, once the inclination angle is greater than 0° (IV, Fig. 7b), the EOR effect monitored in grooves with a large entry angle can be applied, namely difficulty in forming JNP adsorption film and inadequate driving force for the JNP to invade into the groove. In the extreme case where ridges are sharp tips, in other words with zero *S*, JNPs can directly adsorb on the sidewall of the groove, which is greatly beneficial to the formation of the JNPs adsorption film and the optimal EOR effect.

It should be emphasized that this work is only the first step in understanding the complex JNPs displacement behavior on the rough surface. In future work, more influencing factors affecting such displacement process should be studied, such as the displacement velocity, surface properties, size, the zeta potential of JNPs, etc. Also, all-atom simulations using real solid surface structures will reveal more detailed mechanisms (Liu et al., 2022). Moreover, machine learning could be an effective tool to clarify the complicated oil displacement effect under the combination of various rough surface parameters. What is even more challenging is to quantitatively link the surface roughness parameters of the actual reservoir with the displacement effect and explore the macro influencing factors in the reservoir like porosity, permeability, and the remaining oil saturation. So that the precise screening can be realized in the application of JNP in EOR.

5. Conclusions

MD simulations are employed to study the effects of surface roughness on oil displacement by JNPs. The results provide an improved understanding of the previously reported 'adsorption invasion process' of JNPs in displacing trapped oil. The weakly to moderately hydrophobic surface facilitates the progress of dynamics local wettability alteration and is thus suitable for efficient displacement.

The four geometric factors play specific roles in the oil displacement process and the subsequent EOR results. The tip length of the ridge determines the amount of JNPs accumulated on the surface, and further the formation of the JNPs adsorption film in the groove. As the tip length of the ridge reaches a threshold, the properties of the resulting JNPs adsorption film and the EOR effects stabilize, while the required oil displacement time decreases. Although the EOR effect of entry and exit angle of the groove is found similar (small value is the preference), the underlying mechanisms are different. The entry angle of the groove affects the size of the JNPs adsorption film and thus the wettability alteration on the sidewall of the groove, while the exit angle affects the amount of un-recovered trapped oil at the exit side of the groove.

Lastly, the aspect ratio of the groove exerts a huge impact on the morphology of the oil-water interface in the groove. The oil-water interface can curve to reach the bottom of the groove with a large aspect ratio, which results in an excellent oil displacement effect. High oil displacement performance by JNPs is expected in shallow grooves on rough surfaces. Moreover, compared to the entry and exit angle, the aspect ratio of the groove plays a dominating role in the overall EOR effect as long as the tip length of the rough ridge approaches an effective threshold. Our findings deepen the understanding of the displacement of residual oil on the rough interface by injection of nanofluid with JNPs. This study not only guides the application of JNPs in EOR but also serves as an inspiration to the related research on the two-phase flow phenomena on the rough surface.

Abbreviations

Term	Meaning
JNPs	Janus nanoparticles
EOR	Enhance oil recovery
DPD	Dissipative particle dynamics
MD	Molecular dynamics
S	Tip length of the ridge
α	Entry angle
β	Exit angle
A	Aspect ratio of the groove
W	Groove width

H	Groove depth
d	Diameter of JNPs
mW	Monoatomic water
TraPPE-UA	The Transferable Potentials for Phase Equilibria united-atom
SW	Stillinger-Weber
LJ	Lennard-Jones
NEMD	Non-equilibrium molecular dynamics
D	Averaged absolute coordinate of the adsorbed JNP
$R_{\text{hydrophilic}}$	Area of surface wettability alteration by individual JNP
φ	Surface coverage ratio

Appendix A. Supplementary data

Supplementary data to this article can be found online at https://doi.org/10.1016/j.petsci.2023.02.006.

References

Ahmadi, M., Chen, Z., 2021. Comprehensive molecular scale modeling of anionic surfactant-asphaltene interactions. Fuel 288, 119729. https://doi.org/10.1016/j.fuel.2020.119729.

Chang, Y., Jiang, H., Li, J., et al., 2016. The study on crestal injection for fault block reservoir withhigh dip and low permeability. Sci. Technol. Eng. 16, 179–183. https://doi.org/10.3969/j.issn.1671-1815.2016.33.032 (in Chinese).

Chang, Y., Xiao, S., Fu, Y., et al., 2021. Nanomechanical characteristics of trapped oil droplets with nanoparticles: a molecular dynamics simulation. J. Petrol. Sci. Eng. 203, 108649. https://doi.org/10.1016/j.petrol.2021.108649.

Chang, Y., Xiao, S., Ma, R., et al., 2022a. Displacement dynamics of trapped oil in rough channels driven by nanofluids. Fuel 314, 122760. https://doi.org/10.1016/j.fuel.2021.122760.

Chang, Y., Xiao, S., Ma, R., et al., 2022b. Atomistic insight into oil displacement on rough surface by Janus nanoparticles. Energy 245, 123264. https://doi.org/10.1016/j.energy.2022.123264.

Chen, Z., Qian, J., Zhan, H., et al., 2017. Effect of roughness on water flow through a synthetic single rough fracture. Environ. Earth Sci. 76, 186. https://doi.org/10.1007/s12665-017-6470-7.

Durret, J., Szkutnik, P.-D., Frolet, N., et al., 2018. Superhydrophobic polymeric films with hierarchical structures produced by nanoimprint (NIL) and plasma roughening. Appl. Surf. Sci. 445, 97–106. https://doi.org/10.1016/j.apsusc.2018.03.010.

Fang, T., Zhang, Y., Ma, R., et al., 2019. Oil extraction mechanism in CO2 flooding from rough surface: molecular dynamics simulation. Appl. Surf. Sci. 494, 80–86. https://doi.org/10.1016/j.apsusc.2019.07.190.

Giraldo, L.J., Gallego, J., Villegas, J.P., et al., 2019. Enhanced waterflooding with NiO/SiO2 0-D Janus nanoparticles at low concentration. J. Petrol. Sci. Eng. 174, 40–48. https://doi.org/10.1016/j.petrol.2018.11.007.

Harrison, A., Cracknell, R., Krueger-Venus, J., et al., 2014. Branched versus linear alkane adsorption in carbonaceous slit pores. Adsorption 20, 427–437. https://doi.org/10.1007/s10450-013-9589-1.

Hoover, W.G., 1985. Canonical dynamics: equilibrium phase-space distributions. Phys. Rev. A 31, 1695. https://doi.org/10.1103/PhysRevA.31.1695.

Jia, C., 2020. Development challenges and future scientific and technological researches in China's petroleum industry upstream. Acta Petrol. Sin. 41, 1445–1464. https://doi.org/10.7623/syxb202012001 (in Chinese).

Jia, X., Luo, J., Wang, P., et al., 2021. Synthesis of dumbbell-like SiO2 nanoparticles with amphiphilic properties in aqueous phase. Chin. J. Inorg. Chem. 37, 653–660. https://doi.org/10.11862/CJIC.2021.061 (in Chinese).

Kang, Y., Tian, J., Luo, P., et al., 2020. Technical bottlenecks and development strategies of enhancing recovery for tight oil reservoirs. Acta Petrol. Sin. 41, 467–477. https://doi.org/10.7623/syxb202004009 (in Chinese).

Kondratyuk, P., Wang, Y., Johnson, J.K., et al., 2005. Observation of a one-dimensional adsorption site on carbon nanotubes: adsorption of alkanes of different molecular lengths. J. Phys. Chem. B 109, 20999–21005. https://doi.org/10.1021/jp0582078.

Lalegani, F., Saffarian, M.R., Moradi, A., et al., 2018. Effects of different roughness elements on friction and pressure drop of laminar flow in microchannels. Int. J. Heat Fluid Flow 28, 1664–1683. https://doi.org/10.1108/hff-04-2017-0140.

Li, S., Guo, P., Dai, L., et al., 2000. Strenthen gas injection for enhanced oil recovery. J. Southwest Petrol. Univ. 22, 41. https://doi.org/10.3863/j.issn.1000-2634.2000.03.011 (in Chinese).

Li, W., Nan, Y., You, Q., et al., 2020. Effects of salts and silica nanoparticles on oil-brine interfacial properties under hydrocarbon reservoir conditions: a molecular dynamics simulation study. J. Mol. Liq. 305, 112860. https://doi.org/10.1016/j.molliq.2020.112860.

Liang, F., Liu, B., Cao, Z., et al., 2017. Janus colloids toward interfacial engineering. Langmuir 34, 4123–4131. https://doi.org/10.1021/acs.langmuir.7b02308.

Liang, T., Hou, J.-R., Qu, M., et al., 2021. Application of nanomaterial for enhanced oil recovery. Petrol. Sci. 19 (2), 882–899. https://doi.org/10.1016/j.petsci.2021.11.011.

Liu, J., Yang, Y., Sun, S., et al., 2022. Flow behaviors of shale oil in kerogen slit by molecular dynamics simulation. Chem. Eng. J. 434, 134682. https://doi.org/10.1016/j.cej.2022.134682.

Liu, P., Li, X., Yu, H., et al., 2020. Functional janus-SiO2 nanoparticles prepared by a novel "cut the gordian knot" method and their potential application for enhanced oil recovery. ACS Appl. Mater. Interfaces 12, 24201–24208. https://doi.org/10.1021/acsami.0c01593.

Luo, D., Wang, F., Zhu, J., et al., 2016. Nanofluid of graphene-based amphiphilic Janus nanosheets for tertiary or enhanced oil recovery: high performance at low concentration. Proc. Natl. Acad. Sci. USA 113, 7711–7716. https://doi.org/10.1073/pnas.160813511.

Luu, X.C., Striolo, A., 2014. Ellipsoidal Janus nanoparticles assembled at spherical oil/water interfaces. J. Phys. Chem. B 118, 13737–13743. https://doi.org/10.1021/jp5085422.

Martin, M.G., Siepmann, J.I., 1998. Transferable potentials for phase equilibria. 1. United-atom description of n-alkanes. J. Phys. Chem. B 102, 2569–2577. https://doi.org/10.1021/jp972543+.

Molinero, V., Moore, E.B., 2009. Water modeled as an intermediate element between carbon and silicon. J. Phys. Chem. B 113, 4008–4016. https://doi.org/10.1021/jp805227c.

Niu, D., Tang, G., 2014. Static and dynamic behavior of water droplet on solid surfaces with pillar-type nanostructures from molecular dynamics simulation. Int. J. Heat Mass Tran. 79, 647–654. https://doi.org/10.1016/j.ijheatmasstransfer.2014.08.047.

Plimpton, S., 1995. Fast parallel algorithms for short-range molecular dynamics. J. Comput. Phys. 117, 1–19. https://doi.org/10.1006/jcph.1995.1039.

Qian, B., Li, M., 2018. The energy structure continues to diversify with the growth of energy demand——interpretation of the 2018 World Energy Statistical Yearbook. Econ. Anal. China. Petrol. Chem. Ind. 8, 51–54. CNKI:SUN:SYFX.0.2018-08-023 (in Chinese).

Savoy, E.S., Escobedo, F.A., 2012. Molecular simulations of wetting of a rough surface by an oily fluid: effect of topology, chemistry, and droplet size on wetting transition rates. Langmuir 28, 3412–3419. https://doi.org/10.1021/la203921h.

Shi, F., Wu, J., Zhao, B., et al., 2019. Structural characterization and oil displacement performance of Janus micro-nanocapsules. J. Silicate 11. https://doi.org/10.14062/j.issn.0454-5648.2019.11.20.

Song, F., Ma, L., Fan, J., et al., 2018. Wetting behaviors of a nano-droplet on a rough solid substrate under perpendicular electric field. Nanomaterials 8, 340. https://doi.org/10.3390/nano8050340.

Stukowski, A., 2009. Visualization and analysis of atomistic simulation data with OVITO–the Open Visualization Tool. Model. Simulat. Mater. Sci. Eng. 18, 015012. https://doi.org/10.1088/0965-0393/18/1/015012.

Sun, D., Ye, Y., Liang, F., et al., 2021. Some recent advances in Janus particulate emulsifiers. CIE J. 72, 6203–6215. https://doi.org/10.11949/0438-1157.20211277.

Sun, X., Dong, M., Zhang, Y., et al., 2015. Enhanced heavy oil recovery in thin reservoirs using foamy oil-assisted methane huff-n-puff method. Fuel 159, 962–973. https://doi.org/10.1016/j.fuel.2015.07.056.

Wang, G., Wang, Y., Wang, J., et al., 2017. Kinetic Monte Carlo study on the evolution of silicon surface roughness under hydrogen thermal treatment. Appl. Surf. Sci. 414, 361–364. https://doi.org/10.1016/j.apsusc.2017.04.002.

Wang, X., Xiao, S., Zhang, Z., et al., 2019. Transportation of Janus nanoparticles in confined nanochannels: a molecular dynamics simulation. Environ. Sci. Nano 6, 2810–2819. https://doi.org/10.1039/C9EN00314B.

Wu, H., Gao, K., Lu, Y., et al., 2020a. Silica-based amphiphilic Janus nanofluid with improved interfacial properties for enhanced oil recovery. Colloids Surf. Physicochem. Eng. Aspects 586, 124162. https://doi.org/10.1016/j.colsurfa.2019.124162.

Wu, J., Shi, F., Zhao, Y., et al., 2020b. Research progress of functional nano oil displacement agents. J. Northwest. Polytech. Univ. 44 (5), 70–75. https://doi.org/10.3969/j.issn.2095-4107.2020.05.001 (in Chinese).

Xiang, W., Zhao, S., Song, X., et al., 2017. Amphiphilic nanosheet self-assembly at the water/oil interface: computer simulations. Phys. Chem. Chem. Phys. 19, 7576–7586. https://doi.org/10.1039/C6CP08654C.

Xie, J.F., Cao, B.Y., 2016. Nanochannel flow past permeable walls via molecular dynamics. AIP Adv. 6, 075307. https://doi.org/10.1063/1.4959022.

Yaghoubi, H., Foroutan, M., 2018. Molecular investigation of the wettability of rough surfaces using molecular dynamics simulation. Phys. Chem. Chem. Phys. 20, 22308–22319. https://doi.org/10.1039/C8CP03762K.

Yin, T., Yang, Z., Dong, Z., et al., 2019. Physicochemical properties and potential applications of silica-based amphiphilic Janus nanosheets for enhanced oil recovery. Fuel 237, 344–351. https://doi.org/10.1016/j.fuel.2018.10.028.

Yin, T., Yang, Z., Zhang, F., et al., 2021. Assembly and mechanical response of amphiphilic Janus nanosheets at oil-water interfaces. J. Colloid Interface Sci. 583, 214–221. https://doi.org/10.1016/j.jcis.2020.09.026.

Zhang, X., Guo, J., Gao, C., et al., 2022. Application progress of nanoparticle enhancement for enhanced oil recovery, 01 Oilfield Chem. 39, 186–190. https://doi.org/10.19346/j.cnki.1000-4092.2022.01.031.

Zhang, Y., 2016. Effect of wall surface roughness on mass transfer in a nano channel. Int. J. Heat Mass Tran. 100, 295–302. https://doi.org/10.1016/j.ijheatmasstransfer.2016.04.097.

Zhao, J., Yao, G., Ramisetti, S.B., et al., 2019. Molecular dynamics investigation of substrate wettability alteration and oil transport in a calcite nanopore. Fuel 239, 1149–1161. https://doi.org/10.1016/j.fuel.2018.11.089.